Journal of Alloys and Compounds 503 (2010) 133–137

Contents lists available at ScienceDirect

Journal of Alloys and Compounds

journal homepage: www.elsevier.com/locate/jallcom

Mixing up-conversion excitation behaviors in Er^{3+}/Yb^{3+}-codoped aluminum germanate glasses for visible waveguide devices

H. Gong[a,b], L. Lin[c], X. Zhao[a], E.Y.B. Pun[b], D.L. Yang[a,b], H. Lin[a,b,*]

[a] Faculty of Chemical Engineering and Materials, Dalian Polytechnic University, Dalian 116034, PR China
[b] Department of Electronic Engineering, City University of Hong Kong, Tat Chee Avenue, Kowloon, Hong Kong, PR China
[c] Dalian Medical University, Dalian 116027, PR China

ARTICLE INFO

Article history:
Received 26 January 2010
Received in revised form 29 April 2010
Accepted 29 April 2010
Available online 5 May 2010

Keywords:
Germanate glasses
Rare-earth ions
Mixing up-conversion process
Visible waveguide

ABSTRACT

A mixing up-conversion excitation phenomenon in Er^{3+}/Yb^{3+}-codoped aluminum germanate (Na_2O–MgO–Al_2O_3–GeO_2, NMAG for short) glasses for K^+–Na^+ ion-exchanged waveguides was observed and characterized. The green and red up-conversion luminescence of Er^{3+} is due to a two-photon excitation process under low-power excitation of a 974 nm diode laser, however, with increasing the pumping power, the green emission turns to follow a combination of two- and three-photon excitation effects while the red one still agrees with a two-photon excitation law. Under high-power pumping, owing to potential thermal effect, the population ratio between the $^2H_{11/2}$ and $^4S_{3/2}$ levels adjusts acutely, which results in a distinct exhibition in $^2H_{11/2} \rightarrow {}^4I_{15/2}$ and $^4S_{3/2} \rightarrow {}^4I_{15/2}$ emission transitions. Green transmission trace has been observed in K^+–Na^+ ion-exchanged Er^{3+}/Yb^{3+}-codoped NMAG glass waveguide and it provides an original reference in developing visible waveguide amplifiers and lasers.

1. Introduction

High-density green light is independent source in three-dimensional display, and also has excellent application prospect in high-density optical storage and visible lasers and amplifiers [1–11]. Up to now, green up-conversion fluorescence produced in rare-earth (RE) ions doped substrates has attracted much attention due to the high color purity in the absence of disturbance from near-infrared (NIR) pump sources. In green up-conversion emitting centers, Er^{3+} and Ho^{3+} ions act as two outstanding roles, and especially, Er^{3+} exhibits more attractive properties owing to the powerful commercial lasers with wavelength ~980 nm [12–28]. Among the various Er^{3+} doped materials, transparent glasses are identified to be more practical substrates for devices due to higher visible light transmittance, which is helpful to reduce transmission loss. Compared with non-oxide glasses, oxide glasses possess higher phonon energy and up-conversion emissions are considered to be inefficient. However, the chemical stability in oxide glasses is perfect and it is a key factor in actual device fabrication. Hence, designing and optimizing stable glass substrate with lower phonon energy is a precondition in developing high-quality up-conversion devices.

In addition, structural selection of optical devices between optical fiber and planar waveguide corresponds to different results. As is known, up-conversion fluorescence is highly influenced by the RE ion concentration, and high-concentration doping (below quenching concentration) is associated with high-intensity emission. For RE doped optical fiber, the doping concentration is limited to less than 500 ppm due to the restriction of the fiber defect control and the difference of the refractive index in the bulk and surface. In contrast to glass fibers, high-concentration doping is usually adopted in waveguide substrate glasses without any problem, and thus the waveguide is a preferable device form in achieving efficient up-conversion emission.

In this work, investigations on up-conversion fluorescence have been carried out in Er^{3+}/Yb^{3+}-codoped low phonon energy aluminum germanate (Na_2O–MgO–Al_2O_3–GeO_2, NMAG for short) glasses, which are available for waveguides. A mixing up-conversion excitation phenomenon of green fluorescence was observed, and the similar phenomenon was discovered and discussed only in high phonon-energy glasses and crystals before [29–35]. To further expose the characteristic of green light, the differentiation between $^2H_{11/2} \rightarrow {}^4I_{15/2}$ and $^4S_{3/2} \rightarrow {}^4I_{15/2}$ emission transitions was detailed investigated. Owing to the attractive green fluorescence, further attempt on waveguide was carried out. Green transmission trace was successfully obtained in K^+–Na^+ ion-exchanged Er^{3+}/Yb^{3+}-codoped NMAG glass waveguide, which

* Corresponding author at: Faculty of Chemical Engineering and Materials, Dalian Polytechnic University, Dalian 116034, PR China.
Tel.: +86 411 86323097; fax: +86 411 86322228.
E-mail address: lhai8686@yahoo.com (H. Lin).

0925-8388/$ – see front matter © 2010 Elsevier B.V. All rights reserved.
doi:10.1016/j.jallcom.2010.04.216

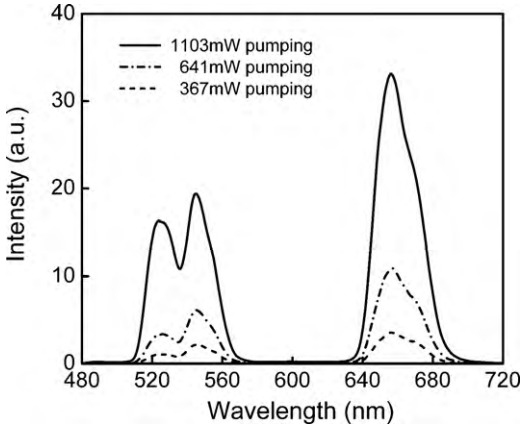

Fig. 1. Up-conversion spectra of 1 wt% Er_2O_3 and 2 wt% Yb_2O_3 codoped NMAG glasses.

provides an original reference in developing up-conversion waveguide devices.

2. Experimental details

Er^{3+}/Yb^{3+}-codoped NMAG glasses were prepared from high-purity Na_2CO_3, MgO, Al_2O_3, GeO_2, Er_2O_3 and Yb_2O_3 powders according to the molar host composition 23%Na_2O–3%MgO–22%Al_2O_3–52%GeO_2. The 1 wt% of Er_2O_3 and 2 wt% of Yb_2O_3 compounds were selected. The detailed melting procedure for NMAG glasses was presented in Ref. [17]. For optical measurements, the annealed glass samples were sliced and polished to pieces with two parallel sides. Visible up-conversion emissions were recorded by a PerkinElmer LS 55 luminescence spectrometer with a R928 photomultiplier detector while a 974 nm wavelength multimode diode laser was adopted as the pump source. In addition, the fluorescence decay curve of $^4S_{3/2}$ level was determined using a Horiba Jobin Yvon FL3-21-iHR-TCSPC spectrometer completed with a pulsed xenon lamp and a R928 photomultiplier detector. The corresponding lifetime was deconvolved from the decay curve by operating the measurement software.

The Er^{3+}/Yb^{3+}-codoped NMAG glass substrates were optically polished and cleaned before the fabrication of K^+–Na^+ ion-exchanged waveguides. Ion-exchange processes were carried out in 390 °C KNO_3 molten bath during different ion-exchange periods. Metricon 2010 prism coupler was used to determine the effective indices and the number of guided modes in ion-exchanged slab waveguide. For channel waveguide fabrication, a 200-nm-thick aluminum film was deposited onto the glass surface using an Edwards Auto 306 thermal evaporator, and then groups of 6-μm-wide channels were opened by a standard micro-fabrication process and wet chemical etching method. After the thermal ion-exchanged operation, the aluminum film was removed and the two end-facets of the waveguides were polished. A 975 nm single-mode laser beam was coupled into the 1.6 cm long Er^{3+}/Yb^{3+}-codoped NMAG glass waveguide channel, and the generation and transmission of up-conversion fluorescence in the devices were observed.

3. Results and discussion

3.1. Green and red up-conversion emissions of Er^{3+}

Up-conversion emission spectra of Er^{3+}/Yb^{3+}-codoped NMAG glasses are shown in Fig. 1 and the visible up-conversion fluorescence includes green and red emissions of Er^{3+} ions. The overlapped green emission band is attributed to the combination of $^2H_{11/2} \rightarrow {}^4I_{15/2}$ and $^4S_{3/2} \rightarrow {}^4I_{15/2}$ transitions, and the red one corresponds to the $^4F_{9/2} \rightarrow {}^4I_{15/2}$ transition. Table 1 presents the measured lifetime τ_m and the quantum efficiency η_q of the $^4S_{3/2}$ level in NMAG and other various glasses. In NMAG glass, the lifetime τ_m under 521 nm wavelength excitation is measured to be 13.6 μs, which is longer than those reported in lead–tellurium–germanate, fluorophosphate, $Na_2O{\cdot}Ca_3Al_2Ge_3O_{12}$, germanate, lead–germanate and silicate glasses, but shorter than the values in CaO–Ga_2O_3–GeO_2 and aluminate glasses [36–39], providing a metastable state to achieve efficient up-conversion emission and potential further photon absorption. In addition, the quantum efficiency η_q of the $^4S_{3/2}$ level in NMAG glass can be

Table 1
Measured lifetime and quantum efficiency of the $^4S_{3/2}$ level in different types of glasses.

Glasses [Ref.]	τ_m of $^4S_{3/2}$ (μs)	η_q of $^4S_{3/2}$ (%)
NMAG glass [this work]	13.6	1.43
CaO–Ga_2O_3–GeO_2 glass [36]	22.0	7.17
Aluminate glass [37]	15.6	3.27
Lead–tellurium–germanate glass [38]	13.0	3.82
Fluorophosphate glass [37]	12.6	1.77
$Na_2O{\cdot}Ca_3Al_2Ge_3O_{12}$ glass [39]	11.7	0.85
Germanate glass [37]	7.3	0.44
Lead–germanate glass [38]	7.2	0.92
Silicate glass [37]	0.7	0.08

derived by $\eta_q = \tau_m/\tau_{cal}$ (τ_{cal} is the calculated lifetime), and the value is calculated to be 1.43%, which is higher than the values in $Na_2O{\cdot}Ca_3Al_2Ge_3O_{12}$, germanate, lead–germanate and silicate glasses [36–39]. The fitted slopes of the log–log plots for the dependence of integrated up-conversion emission intensity on excitation intensity are presented in Fig. 2. The slopes of the green fluorescence are 1.81 and 2.51 under low-power and high-power pumping conditions, respectively, and which of the red one maintains 1.94 in both cases. Based on the slopes, the green fluorescence is due to a two-photon excitation process under low-power excitation and a combined effect of two- and three-photon processes under high-power excitation, respectively, and the red emission follows a two-photon excitation law all the while. The exhibition of green fluorescence in this work is quite different from the behaviors in several other Er^{3+}/Yb^{3+}-codoped systems, in which the slope of green fluorescence is close to about 2 under low-power excitation, and can start to decrease under high-power excitation because of the saturation effects [40,41]. Thus, interests in further investigation were aroused due to the special phenomenon of green fluorescence.

Fig. 3 exhibits the energy level diagram of Er^{3+} and Yb^{3+} in NMAG glasses [42–47]. Under low-power excitation of 974 nm laser, for $^4F_{9/2} \rightarrow {}^4I_{15/2}$ transition, Er^{3+} ions are excited to the $^4I_{11/2}$ level by the ground state absorption (GSA) and the energy transfer (ET) from Yb^{3+}, and then partly relax nonradiatively to the $^4I_{13/2}$ level. Then, a part of them move to the $^4F_{9/2}$ level by means of the second ET

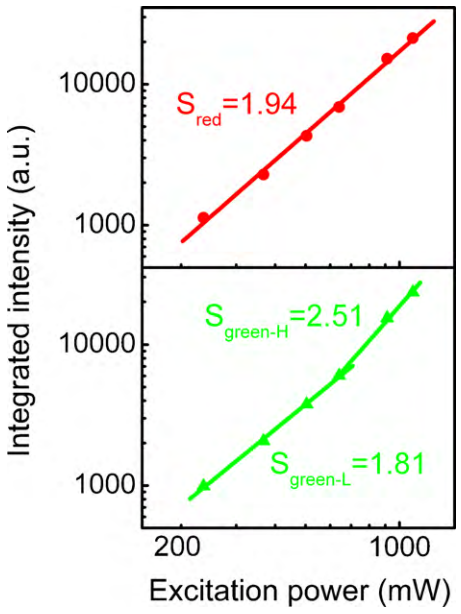

Fig. 2. Dependence of integrated up-conversion emission intensity on excitation power under 974 nm wavelength laser excitation for 1 wt% Er_2O_3 and 2 wt% Yb_2O_3 codoped NMAG glasses.

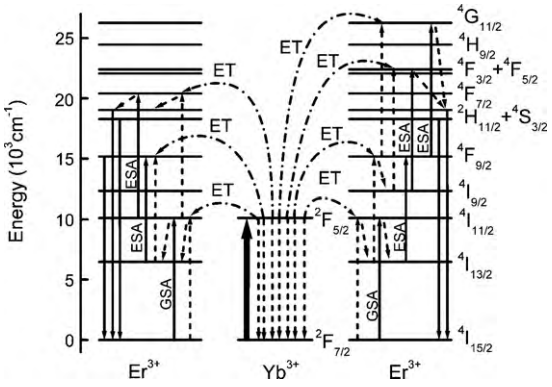

Fig. 3. Energy-level diagram of Er^{3+} and Yb^{3+} in NMAG glasses. Left: The two-photon excitation mechanism of red and green lights under 974 nm laser excitation. Right: The possible three-photon excitation mechanism of green light under 974 nm laser excitation.

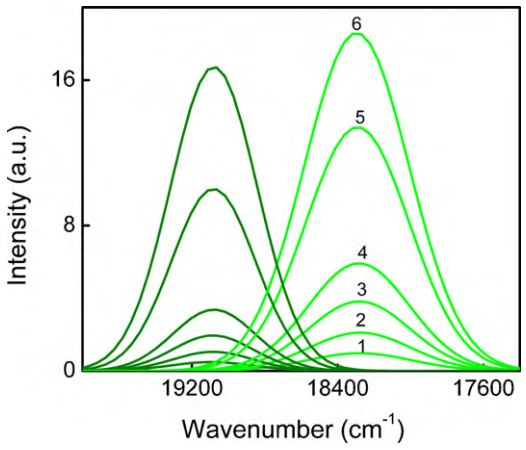

Fig. 4. Gaussian-resolved green emission bands derived from up-conversion spectra recorded under different 974 nm laser excitation powers. Curves 1, 2, 3, 4, 5 and 6 correspond to the laser powers of 236, 367, 504, 641, 913 and 1103 mW, respectively.

and the excited state absorption (ESA) processes, and subsequently relax radiatively to the ground state $^4I_{15/2}$. On the other hand, for $^2H_{11/2} \rightarrow {}^4I_{15/2}$ and $^4S_{3/2} \rightarrow {}^4I_{15/2}$ transitions, the following two processes occur. First, Er^{3+} ions are excited from the ground state $^4I_{15/2}$ to the $^4I_{11/2}$ level. Second, the Er^{3+} ions at the $^4I_{11/2}$ level are excited to the $^4F_{7/2}$ level by the ET and ESA processes, and then relax nonradiatively to the next lower $^2H_{11/2}$ and $^4S_{3/2}$ levels due to the small energy gap. The Er^{3+} ions at the $^2H_{11/2}$ and $^4S_{3/2}$ levels then relax radiatively to the ground state $^4I_{15/2}$ and thus green fluorescence was observed.

With excitation power increasing, the up-conversion excitation mechanism of red emission remains the same as that under low-power excitation. However, for green emissions, additional three-photon process occurs besides the two-photon process mentioned above. Some of the ions at the $^4F_{9/2}$ level are excited to the $^4G_{11/2}$ level by the third ET from Yb^{3+} and ESA:

$$^4F_{9/2}(Er^{3+}) + {}^2F_{5/2}(Yb^{3+}) \rightarrow {}^4G_{11/2}(Er^{3+}) + {}^2F_{7/2}(Yb^{3+}) \quad (1a)$$

$$^4F_{9/2}(Er^{3+}) + \text{photon} \rightarrow {}^4G_{11/2}(Er^{3+}) \quad (1b)$$

and then populate the $^2H_{11/2}$ and $^4S_{3/2}$ levels by nonradiative relaxation. Another possibility is that some ions at the $^4F_{9/2}$ state relax nonradiatively to the $^4I_{9/2}$ level, and then a part of them arrive at the $^4F_{3/2}$ and $^4F_{5/2}$ levels by ET from Yb^{3+} and ESA:

$$^4I_{9/2}(Er^{3+}) + {}^2F_{5/2}(Yb^{3+}) \rightarrow ({}^4F_{3/2} + {}^4F_{5/2})(Er^{3+}) + {}^2F_{7/2}(Yb^{3+}) \quad (2a)$$

$$^4I_{9/2}(Er^{3+}) + \text{photon} \rightarrow ({}^4F_{3/2} + {}^4F_{5/2})(Er^{3+}) \quad (2b)$$

Subsequently, the excited ions at the $^4F_{3/2}$ and $^4F_{5/2}$ levels relax nonradiatively to the $^2H_{11/2}$ and $^4S_{3/2}$ levels.

Due to the attractiveness of the mix-mechanism up-conversion behaviors, further investigation on green fluorescence of Er^{3+} has been done. Two Gaussian-resolved green emission bands, corresponding to $^2H_{11/2} \rightarrow {}^4I_{15/2}$ and $^4S_{3/2} \rightarrow {}^4I_{15/2}$ transitions and locating at ~523 and ~545 nm, are shown in Fig. 4. The fitted slopes of the log–log plots for the dependence of integrated emission intensity on laser pumping power are shown in Fig. 5. At low pumping powers, the slopes of 523 and 545 nm green emissions are both ~2, and at high pumping powers, the values become 3.06 and 2.20, respectively, exhibiting a distinction between $^2H_{11/2} \rightarrow {}^4I_{15/2}$ and $^4S_{3/2} \rightarrow {}^4I_{15/2}$ emission transitions under high-power excitation. As is known, the integrated intensity ratio of two green emission bands is closely related to the temperature, which is given by [48,49]:

$$\delta = \frac{I_{523\,\text{nm}}}{I_{545\,\text{nm}}} = \frac{N(^2H_{11/2})}{N(^4S_{3/2})} = \frac{A_s\sigma_s\omega_s}{A_l\sigma_l\omega_l}\exp\left[\frac{-\Delta E}{KT}\right], \quad (3)$$

where $N(^2H_{11/2})$, $N(^4S_{3/2})$ are the numbers of ions on $^2H_{11/2}$ and $^4S_{3/2}$ levels; σ, ω and A are the emission cross section, the angular frequency and the spontaneous transition probability from excited state to the ground state of Er^{3+}, respectively; K is the Boltzmann constant; ΔE is the energy gap between the two thermally linked levels and T is the absolute temperature. The values of the integrated intensity ratio at different excitation power were calculated and presented in Fig. 6. Under low-power pumping (≤504 mW), the integrated intensity ratio remains ~0.40, indicating that the populations of the two green emissions are stably distributed owing to the relatively steady temperature. However, under high-power pumping (>504 mW), an explosive increase of the integrated intensity ratio was captured owing to the increasing temperature of the sample by excitation power enhancing. Due to the potential thermal effect, the population rate of the $^2H_{11/2}$ level increases faster than that of the $^4S_{3/2}$ level, which results in the distinct exhibition in $^2H_{11/2} \rightarrow {}^4I_{15/2}$ and $^4S_{3/2} \rightarrow {}^4I_{15/2}$ emission transitions.

3.2. Ion-exchanged NMAG glass visible waveguide

Up-conversion behaviors discussed above are helpful in developing visible lasers and amplifiers, thus preliminary attempt on visible waveguide fabrication was carried out. In this work, K^+–Na^+ ion-exchanged Er^{3+}/Yb^{3+}-codoped NMAG glass planar waveguide was successfully fabricated. Fig. 7(a) shows the 632.8 nm laser

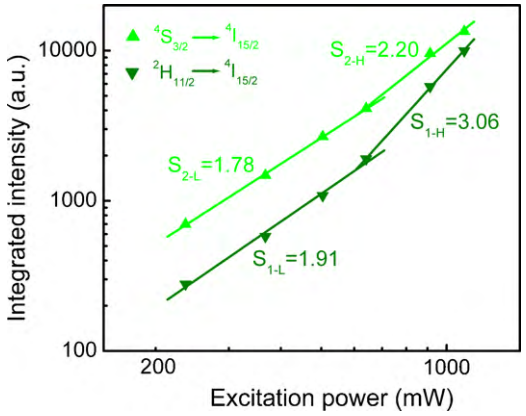

Fig. 5. Dependence of integrated emission intensity on 974 nm wavelength laser excitation power in two Gaussian-resolved green bands. (For interpretation of the references to color in this figure legend, the reader is referred to the web version of the article.)

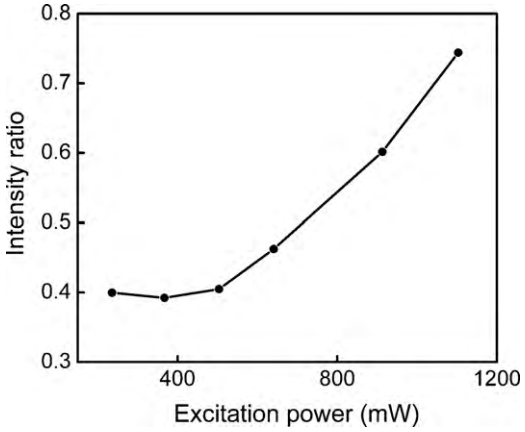

Fig. 6. Dependence of integrated emission intensity ratio of two Gaussian-resolved green bands on 974 nm wavelength laser excitation power.

intensity of reflected light versus index value for 8 h ion-exchanged slab waveguide. Four downward peaks were observed, indicating that four complete modes exist in this slab waveguide. Adopting Inverse-Wentzel–Kramers–Brillouin (IWKB) method, the index profiles as a function of the diffusion depth at 632.8 nm were obtained and depicted in the insert of Fig. 7(a). The surface refractive index of the waveguide n_0 was calculated to be 1.5887 and the refractive index of the glass substrate n_{sub} is 1.5809. Therefore, the maximum refractive index change $\Delta n = n_0 - n_{sub}$ was calculated to be 0.0078. In some cases, single-mode visible waveguide is preferred, and reducing the ion-exchange time can be adopted to achieve the purpose. Fig. 7(b) shows the ion-exchanged slab waveguide for 1 h, and one complete mode was achieved, providing a valuable reference for the development of single-mode visible waveguide lasers and amplifiers.

Based on the parameters of slab waveguide, K^+–Na^+ ion-exchanged Er^{3+}/Yb^{3+}-codoped NMAG glass channel waveguide was successfully prepared. The photograph of up-conversion fluorescence generation and transmission in the channel waveguide are presented in Fig. 8(a) and (b), respectively, and the green transmission trace is clear, bright and compact, which shows a rudiment of visible waveguide devices. Therefore, Er^{3+}/Yb^{3+}-codoped NMAG glasses are considered to be a promising substrate for developing visible lasers and amplifiers, which contains huge application potentials in optical data storage and optical local area networks.

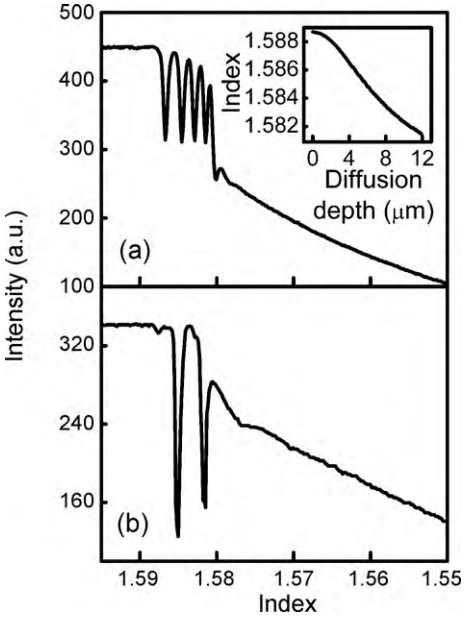

Fig. 7. Intensity of reflected light versus index value. (a) 8 h K^+–Na^+ ion-exchange with 632.8 nm laser source; (b) 1 h K^+–Na^+ ion-exchange with 632.8 nm laser source. Inset in (a) index profile of ion-exchanged slab waveguide.

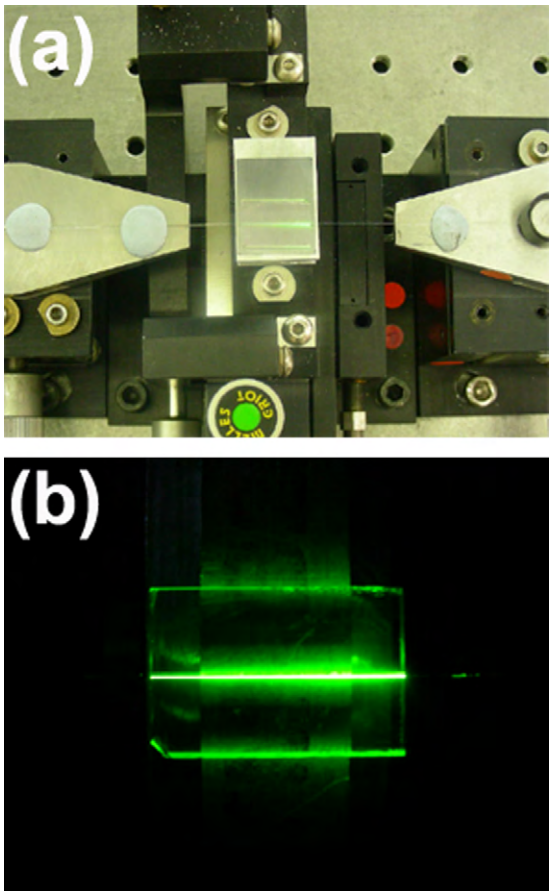

Fig. 8. Photograph of up-conversion fluorescence generation (a) and transmission (b) in 4 h K^+–Na^+ ion-exchanged 1 wt% Er_2O_3 and 2 wt% Yb_2O_3 codoped NMAG glass channel waveguide.

4. Conclusions

In summary, a mixing up-conversion phenomenon in Er^{3+}/Yb^{3+}-codoped NMAG glasses for K^+–Na^+ ion-exchanged waveguides was characterized. Under low-power excitation of a 974 nm wavelength laser diode, efficient two-photon green and red up-conversion luminescence of Er^{3+} was observed. Nevertheless, under high-power pumping, the green emission turns to follow a combination of two- and three-photon excitation law while the red one still agrees with a two-photon excitation process. Due to the potential thermal effect, the population ratio between the $^2H_{11/2}$ and $^4S_{3/2}$ levels adjusts acutely, which results in the distinct exhibitions in $^2H_{11/2} \rightarrow {}^4I_{15/2}$ and $^4S_{3/2} \rightarrow {}^4I_{15/2}$ emission transitions. Green transmission trace observed in K^+–Na^+ ion-exchanged Er^{3+}/Yb^{3+}-codoped NMAG waveguide brings a promising potential in developing visible signal amplifier and high-density green light sources.

Acknowledgements

We would like to acknowledge for the financial support of National Natural Science Foundation of China (60977014), Scientific Research Foundation for Universities from Education Bureau of

Liaoning Province (2009A080) and Research Grants Council of the Hong Kong Special Administrative Region, China (CityU 1197/08).

References

[1] R. Balda, R.I. Merino, J.I. Pena, V.M. Orera, M.A. Arriandiaga, J. Fernandez, Opt. Mater. 31 (2009) 1105.
[2] L.Q. Dong, S.H. Huang, H.Y. Wen, K. Kang, X.X. Duan, J. Rare Earths 27 (2009) 334.
[3] H. Guo, Y.M. Qiao, Opt. Mater. 31 (2009) 583.
[4] N.K. Giri, S.B. Rai, A. Rai, Spectrochim. Acta A 74 (2009) 1115.
[5] W.A. Pisarski, J. Pisarska, R. Lisiecki, L. Grobelny, G. Dominiak-Dzik, W. Ryba-Romanowski, Opt. Mater. 31 (2009) 1781.
[6] H. Tomokatsu, H. Masahiko, N. Masayuki, J. Alloys Compd. 451 (2008) 77.
[7] Z. Jin, Q.H. Nie, T.F. Xu, S.X. Dai, X. Shen, X.H. Zhang, Mater. Chem. Phys. 104 (2007) 62.
[8] K. Kumar, S.B. Rai, D.K. Rai, J. Non-Cryst. Solids 353 (2007) 1383.
[9] A.S.S. de Camargo, J.F. Passatto, L.A. de O. Nunes, E.R. Botero, E.R.M. Andreeta, D. Garcia, J.A. Eiras, Solid State Commun. 137 (2006) 1.
[10] M. Szachowicz, S. Tascu, M.-F. Joubert, P. Moretti, M. Nikl, Opt. Mater. 28 (2006) 162.
[11] T. Danger, J. Koetke, R. Brede, E. Heumann, G. Huber, J. Appl. Phys. 76 (1994) 1413.
[12] J. Ding, Q. Zhang, J. Cheng, X. Liu, G. Lin, J. Qiu, D. Chen, J. Alloys Compd. 495 (2010) 205.
[13] S. Zeng, G. Ren, Q. Yang, J. Alloys Compd. 493 (2010) 476.
[14] Z. Chouahda, J.P. Jouart, T. Duvaut, M. Diaf, J. Phys. Condens. Matter 21 (2009) 245504.
[15] T. Som, B. Karmakar, Opt. Mater. 31 (2009) 609.
[16] D.G. Deng, S.Q. Xu, S.L. Zhao, C.X. Li, H.P. Wang, H.D. Ju, J. Lumin. 129 (2009) 1266.
[17] D.L. Yang, E.Y.B. Pun, B.J. Chen, H. Lin, J. Opt. Soc. Am. B 26 (2009) 357.
[18] Y.Q. Qu, X.G. Kong, Y.J. Sun, Q.H. Zeng, H. Zhang, J. Alloys Compd. 485 (2009) 493.
[19] H.Y. Du, Y.J. Lan, Z.G. Xia, J.Y. Sun, Mater. Res. Bull. 44 (2009) 1660.
[20] P. Haro-Gonzalez, F. Lahoz, J. Gonzalez Platas, J.M. Caceres, S. Gonzalez-Perez, D. Marrero-Lopez, N. Capuj, I.R. Martin, J. Lumin. 128 (2008) 908.
[21] Y.S. Luo, J.H. Zhang, X. Zhang, X.J. Wang, J. Appl. Phys. 103 (2008) 063107.
[22] C. Gheorghe, S. Georgescu, V. Lupei, A. Lupei, A. Ikesue, J. Appl. Phys. 103 (2008) 083116.
[23] P. Joshi, S.X. Shen, A. Jha, J. Appl. Phys. 103 (2008) 083543.
[24] J. Mendez-Ramos, V.D. Rodriguez, V.K. Tikhomirov, J. del-Castillo, A.C. Yanes, Eur. Phys. J. Appl. Phys. 43 (2008) 149.
[25] R. Weber, S. Hampton, P.C. Nordine, T. Key, R. Scheunemann, J. Appl. Phys. 98 (2005) 043521.
[26] S. Georgescu, O. Toma, I. Ivanov, J. Lumin. 114 (2005) 43.
[27] M. Tsuda, K. Soga, H. Inoue, S. Inoue, A. Makishima, J. Appl. Phys. 85 (1999) 29.
[28] Y. Kawamoto, R. Kanno, J. Qiu, J. Mater. Sci. 33 (1998) 63.
[29] X. Wang, G.Y. Shan, K.f. Chao, Y.L. Zhang, R.L. Liu, L.Y. Feng, Q.H. Zeng, Y.J. Sun, Y.C. Liu, X.G. Kong, Mater. Chem. Phys. 99 (2006) 370.
[30] H. Guo, Opt. Mater. 29 (2007) 1840.
[31] X. Zhang, J.H. Yuan, X.R. Liu, J.P. Jouart, G. Mary, Chem. Phys. Lett. 273 (1997) 416.
[32] H.W. Song, B.J. Sun, T. Wang, S.Z. Lu, L.M. Yang, B.J. Chen, X.J. Wang, X.G. Kong, Solid State Commun. 132 (2004) 409.
[33] F. Vetrone, J. Boyer, J.A. Capobianco, A. Speghini, M. Bettinelli, J. Appl. Phys. 96 (2004) 661.
[34] F. Song, G.Y. Zhang, M. Shang, H. Tan, J. Yang, F.Z. Meng, Appl. Phys. Lett. 79 (2001) 1748.
[35] G.Y. Chen, Y. Liu, Z.G. Zhang, B. Aghahadi, G. Somesfalean, Q. Sun, F.P. Wang, Chem. Phys. Lett. 448 (2007) 127.
[36] B.V. Padlyak, W. Ryba-Romanowski, R. Lisiecki, J. Non-Cryst. Solids 354 (2008) 4249.
[37] X. Zou, T. Izumitani, J. Non-Cryst. Solids 162 (1993) 68.
[38] Z. Pan, S.H. Morgan, K. Dyer, A. Ueda, J. Appl. Phys. 79 (1996) 8906.
[39] H. Lin, E.Y.B. Pun, S.Q. Man, X.R. Liu, J. Opt. Soc. Am. B 18 (2001) 602.
[40] M. Pollnau, D.R. Gamelin, S.R. Luthi, H.U. Gudel, M.P. Hehlen, Phys. Rev. B 61 (2000) 3337.
[41] J.F. Suyver, A. Aebischer, S. Garcia-Revilla, P. Gerner, H.U. Gudel, Phys. Rev. B 71 (2005) 125123.
[42] L.A. Gomez, G.S. Maciel, C.B. Araujo, A. Patra, J. Appl. Phys. 103 (2008) 053507.
[43] H. Desirena, E. De la Rosa, A. Shulzgen, S. Shabet, N. Peyghambarian, J. Phys. D: Appl. Phys. 41 (2008) 095102.
[44] G.A. Kumar, E. De la Rosa, H. Desirena, Opt. Commun. 260 (2006) 601.
[45] P. Babu, H.J. Seo, K.H. Jang, K.U. Kumar, C.K. Jayasankar, Chem. Phys. Lett. 445 (2007) 162.
[46] F.A. Bomfim, J.R. Martinelli, L.R.P. Kassab, N.U. Wetter, J.J. Neto, J. Non-Cryst. Solids 354 (2008) 4755.
[47] S. Garcia-Revilla, R. Valiente, Y.E. Romanyuk, M. Pollnau, J. Lumin. 128 (2008) 934.
[48] S.F. Collins, G.W. Baxter, S.A. Wade, T. Sun, K.T.V. Grattan, Z.Y. Zhang, A.W. Palmer, J. Appl. Phys. 84 (1998) 4649.
[49] S.A. Wade, S.F. Collins, G.W. Baxter, Appl. Phys. Rev. 94 (2003) 4743.